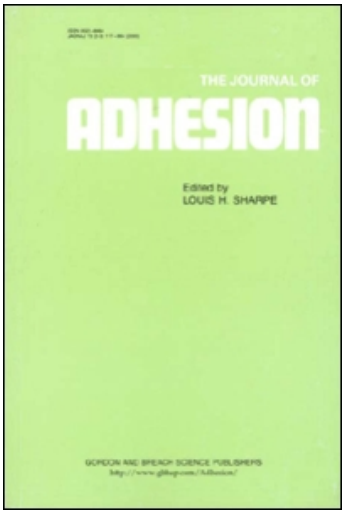

The Journal of Adhesion
Publication details, including instructions for authors and subscription information:
http://www.informaworld.com/smpp/title~content=t713453635

Joint Strength Optimization of Adhesively Bonded Patches

E. A. S. Marques[a]; Lucas F. M. da Silva[a]
[a] Departamento de Engenharia Mecnica e Gestão Industrial, Faculdade de Engenharia, Universidade do Porto, Rua Dr. Roberto Frias, Porto, Portugal

To cite this Article Marques, E. A. S. and da Silva, Lucas F. M.(2008) 'Joint Strength Optimization of Adhesively Bonded Patches', The Journal of Adhesion, 84: 11, 915 — 934
To link to this Article: DOI: 10.1080/00218460802505275
URL: http://dx.doi.org/10.1080/00218460802505275

The Journal of Adhesion, 84:915–934, 2008

ISSN: 0021-8464 print/1545-5823 online
DOI: 10.1080/00218460802505275

Taylor & Francis
Taylor & Francis Group

Joint Strength Optimization of Adhesively Bonded Patches

E. A. S. Marques and Lucas F. M. da Silva
[1]Departamento de Engenharia Mecânica e Gestão Industrial, Faculdade de Engenharia, Universidade do Porto, Rua Dr. Roberto Frias, Porto, Portugal

Aircraft face damage from impact with objects or birds or due to ageing that leads to fatigue cracks. The conventional methods of repairing aircraft metallic structures generally include the use of a plate joined by screws or rivets. Although these methods are efficient in the short term, they introduce stress concentrations leading to the initiation of new cracks that are difficult or impossible to detect by non-destructive methods. For these reasons, it is necessary to develop new methods to improve the behaviour of the structure (especially for long term) and its manufacture cost. One of the solutions that have been studied by the aeronautical industry is the use of patches bonded with structural adhesives. However, adhesively bonded patches have problems of stress concentration at the edges where crack initiation is prone to occur. This problem can be reduced by the use of a taper and a spew fillet at the end of the patch and by the use of a mixed adhesive technique where a ductile adhesive is placed at the edges of the patch. Double strap specimens from 3 mm thick 6063-T6 aluminium alloy sheet were analysed. Aluminium and straps (or patches) with an internal taper, an adhesive spew fillet, and dual adhesives were experimentally tested. The results obtained were explained by a finite element analysis. A taper angle is beneficial only for the brittle adhesive. The use of two adhesives is advantageous for the taperless configuration.

Keywords: Aluminium; Epoxy; Finite element stress analysis; Lap-shear

1. INTRODUCTION

Damage to aircraft is more common than usually thought and appears in various forms of varying severity. “Ramp rash” is a general term used to describe impacts against the surface of the aircraft occurring

Received 19 May 2008; in final form 2 September 2008.
Address correspondence to Lucas F. M. da Silva, Departamento de Engenharia Mechânica e Gestão Industrial, Faculdade de Engenharia, Universidade do Porto, Rua Dr. Roberto Frias 4200-465, Portugal. E-mail: lucas@fe.up.pt

while on the ground. It is usually caused by the maintenance, catering, and baggage handling vehicles in the airport. These impacts, while generally at slow speed, are very concentrated and can produce small and undetectable dents or cracks in the pressurized section of the fuselage. Bird strike is caused by the impact of a bird (or other animal) against the aircraft during flight. Depending on the velocity of the impact and weight of the bird, it can cause variable amounts of damage. This type of damage is usually concentrated in the parts of the aircraft facing directly forward, such as nose cone, cockpit windows, wing leading edges, and vertical and horizontal stabilizer leading edges. Hail damage occurs when the aircraft flies through hail storms. When the hail is big enough, it creates considerable damage on the forward facing zones of the aircraft, the same zones affected by the bird strike. Lightning strike can be intense enough to create small holes or dents in the fuselage. The aeronautical industry also faces problems of ageing such as fatigue and corrosion that require particular attention. The metallic components of the aircraft develop cracks under fatigue loading or stress corrosion. These defects initiate in places of high stress concentration such as rivet holes or non-uniform geometry.

Repair of the damage described above is usually possible by means of a patch applied over the crack. This type of repair is very common and is economically very important, as it allows the safe operation of damaged or older aircraft for an increased amount of time. The current repair technique for aircraft with aluminium fuselages uses riveting to install the repair patch. In this procedure, the aluminium patches are placed over the damaged zone and completely riveted to the aircraft skin. The rivets are evenly distributed over the patch to provide better connection between the patch and fuselage while ensuring lower stress concentrations. Adhesive patches have gained popularity in the last decade as the use of composite parts increased. Suited to almost every material and able to handle complex geometries, this technique is known for its versatility and ease of application. Most aircraft manufacturers have developed portable adhesive repair kits that are easy to carry. This allows the quick repair of stranded and damaged aircraft, making them airworthy and enabling a flight back to a main maintenance base where more resources are available to complete the repair procedure. Hu and Soutis [1] studied a repair procedure in which the damaged material is removed, often by drilling a hole. The remaining material is then cleaned, degreased, and, if necessary, a filler material is applied in the gap. The adhesive and respective repair patches are applied next. The curing is usually done at room temperature but may also require the application of heat using heat blankets or other sources.

In a modern commercial aircraft, the fuselage is not simply for enclosing the interior, it is an integral part of the structure. The aircraft fuselage is comprised of machined aluminium frames, which are connected to each other by beams. These beams and frames are responsible for handling the bulk of the inertial and torsion forces acting on the aircraft during flight. The internal pressure tries to open the fuselage, by introducing tangential traction forces in the fuselage surface. These tangential forces represent the majority of the stress acting on the adhesive joint.

The patch geometry studied here was chosen to suit the repair of a component which suffered cracking damage. The repair patch will act as a bridge between the two sides of the cracked component, transferring the loads over a gap. The adhesive layer acts as the bridge foundations, ensuring the best connection possible between the patch and the adherends. The design of the adhesive layer and the patch is optimized to smooth the transfer of load. The geometry of the joints present in the borders of the patch influences directly the behaviour and durability of the patch. One of the main functions of the joint is to avoid the peeling of the patch. This can be achieved in various ways. In many cases this is done by tapering the surfaces of the patch, but tapering the adhesive is also a possibility. Figure 1 shows the tapering possibilities that have been studied by various authors [2–11]. The main idea is to lower the stiffness at the ends of the overlap for a smoother load transfer. Mixed modulus joints are another possibility to improve the stress distribution and increase the joint strength of

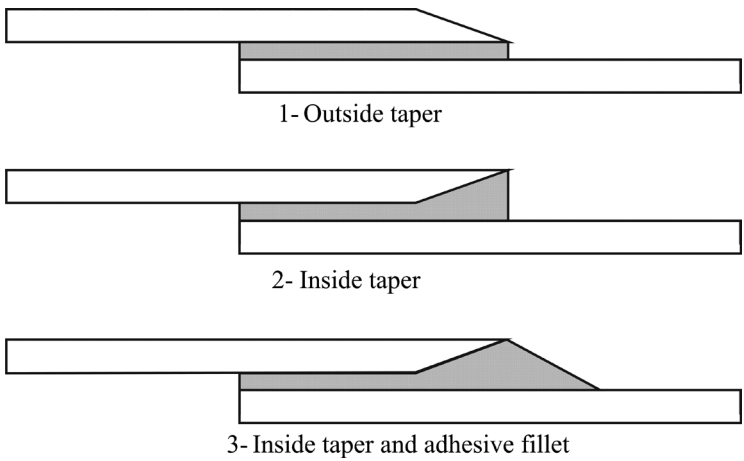

FIGURE 1 Designs of tapered joints.

high modulus adhesives [12–15]. For example, Bouiadjra *et al.* [16] used the mixed modulus technique for the repair of an aluminium structure with a composite patch. The use of a more flexible adhesive at the edge of the patch increases the strength performance of the repair. The technique of using multi-modulus adhesives has been extended by da Silva and Adams to solve the problem of adhesive joints that need to withstand low and high temperatures [17,18].

The objective of the present study was to supplement and expand these previous results. The joint selected for this work was a double butt strap joint, in which two aluminium specimens are interconnected by means of two adhesive layers and two symmetrically placed metal patches. This standard joint is a good simplification of the case encountered in a repair situation. A comparison was made between different patch taper angles. Four different and relatively evenly spaced taper angles were selected to be studied and tested. As shown before, there is already some work in the area, though most works are not focused on aluminium bonding. The gap between the substrates simulates a crack. The mixed adhesive technique was studied with a very brittle adhesive in the middle of the joint and a ductile adhesive at the ends of the patch. Finally, the two methods (tapering and mixed adhesive technique) were combined for testing any synergetic effect.

2. EXPERIMENTAL PROGRAMME

2.1. Materials

Two adhesives were selected, a very stiff and brittle epoxy (Araldite AV138/HV998, Huntsman, Salt Lake City, UT, USA) used in aerospace applications, and a more flexible and ductile epoxy adhesive (Araldite 2015, Huntsman). Uniaxial testing (British standard BS 2782) was done on bulk specimens (three specimens tested for each adhesive) and typical stress-strain curves are shown in Figure 2.

A 6000 series alloy was used to closely represent the aluminium alloys used in the aerospace industry. Although it would be preferable to use a 7000 series, as it is the most used in aeronautical construction, availability constraints lead to the use of 6063 aluminium with T6 heat treatment. This is a very strong aluminium alloy, as the T6 heat treatment raises the tensile strength. It was used in all of the substrates as well as in the reinforcement patches. The properties of the aluminium alloy used are presented in Table 1 [19].

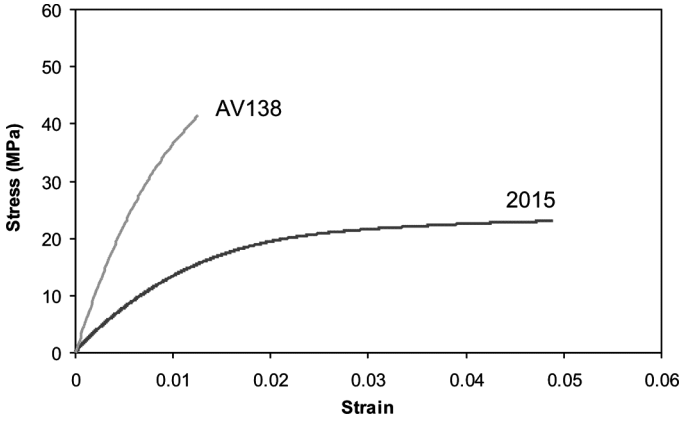

FIGURE 2 Tensile stress-strain curve of adhesives used.

2.2. Specimen Geometry

The double strap joint (DSJ) geometry was selected so as to simulate a crack with a patch. The DSJ had an overlap of 10 mm and a width of 25 mm (see Figure 3a). The overlap length was chosen so that the adherends remain in the elastic range. The load corresponding to the yield of the adherend is given by:

$$F_{\mathrm{s}} = \sigma_{ys} \cdot w \cdot t_{\mathrm{s}}, \tag{1}$$

where F_{s} is the yielding load of the substrate, σ_{ys} is the yield strength of the substrate, w is the joint width, and t_{s} is the substrate thickness. The load corresponding to the total plastic deformation of the adhesive is:

$$F_{\mathrm{a}} = \tau_y \cdot w \cdot 2l, \tag{2}$$

where F_{a} is the failure load of the adhesive, τ_y is the shear yield strength of the adhesive, and l is the overlap length. The substrate will not yield if $F_{\mathrm{s}} > F_{\mathrm{a}}$. This condition (considering the adhesive which has the higher shear strength) means that the overlap length (l) must be lower than 20 mm.

TABLE 1 Tensile Properties of Aluminium [19]

Young's modulus E (GPa)	Poisson's ratio	Tensile yield strength σ_y (MPa)	Tensile strength σ_r (MPa)	Tensile failure strain ε_f (%)
67	0.33	172	206	10

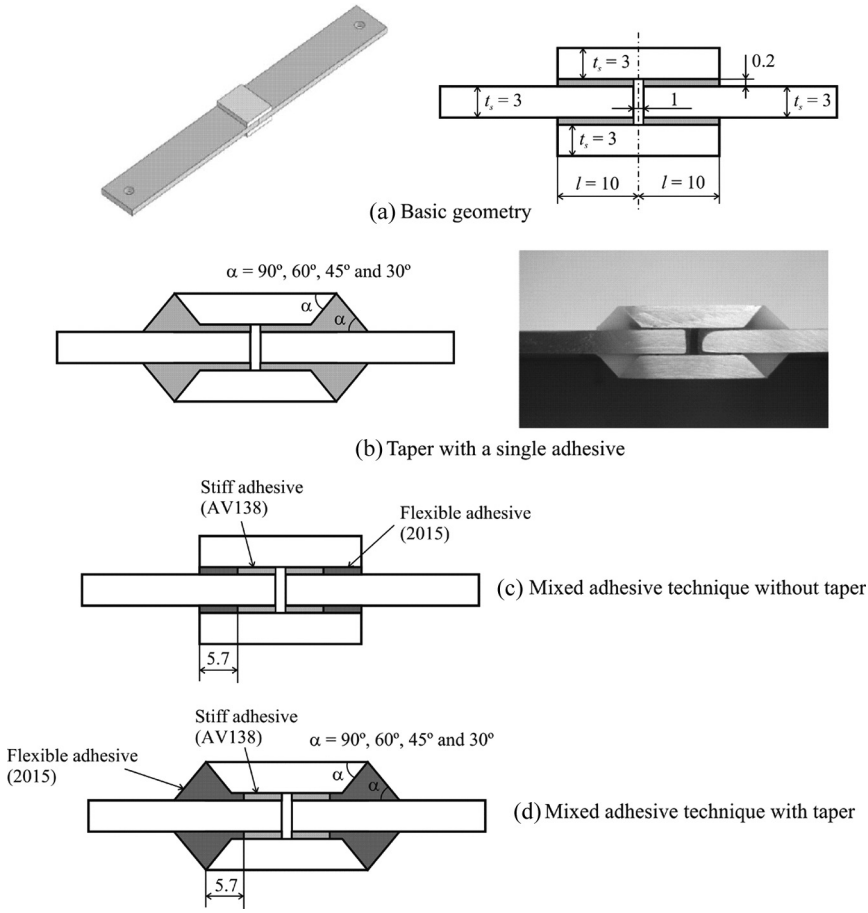

FIGURE 3 Joint geometry (dimensions in mm).

To minimise the high stress concentrations at the end of the patch, three methods were used. The first method consisted in the use of a taper angle. Four different taper angles were considered: 90° (no taper), 60°, 45°, and 30° (see Figure 3b). The second method used a combination of two adhesives, being the brittle AV138 in the middle and the more ductile 2015 at the ends of the patch (see Figure 3c). The third method was a combination of the first and second methods (see Figure 3d). When a combination of two adhesives was used there was the need to select the length that each adhesive would occupy in the adhesive layer. The main concern here was for this length to be the same in all of the different configurations studied to allow direct

comparison of the joint strength. The 30° taper, which is the taper that goes farthest into the overlap, gave a length of 5.7 mm from the end of the patch to the end of the taper. This length was adopted for adhesive 2015 in all the dual adhesive cases to ease the fabrication of the 30° taper case.

2.3. Specimen Manufacture

The specimens were produced in a special mould, which controls the overlap and the adhesive thickness. For the joints with two adhesives, different methods of separation were tested. It was found that the most effective method was the use of a nylon line with the same thickness of the adhesive layer between the adhesives. The nylon line is glued to the substrates using a small amount of cyanoacrylate adhesive. This method gives a very good dimensional control and occupies a very small area when compared with other techniques tested (use of small strips of silicone or Teflon®). The process of construction requires the same mould as the one required to produce DSJ specimens. The mould geometry aligns the substrates, patches, and moulds. The construction must follow a special sequence due to the number of different components that make up each specimen. The sequence is illustrated in Figure 4.

2.4. Test Procedure

The completed specimens were then subjected to a tensile test in an Instron testing machine (High Wycombe, England). The joint

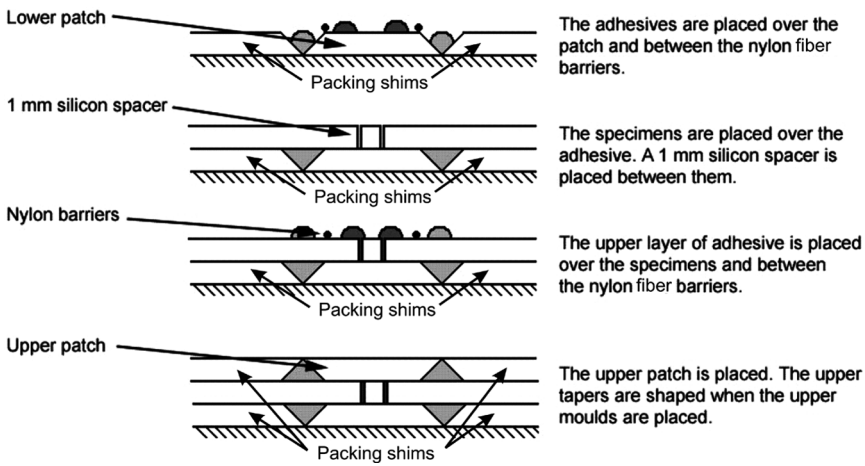

FIGURE 4 Dual adhesive joint construction process.

displacement was measured with a 50 mm extensometer. Three specimens were produced for each taper angle and for each adhesive combination. The specimens were tested under a cross-head displacement rate of 1 mm/min and in typical laboratory ambient conditions (approximately 25°C and 50% relative humidity).

3. EXPERIMENTAL RESULTS

The specimens failed cohesively in the adhesive in all cases. Figure 5 shows a failure surface of a joint with two adhesives and a taper. The crack runs close to the patch/adhesive interface in the area of the taper. The results of tensile testing of the single and dual adhesive specimens are presented in Figure 6 as a function of the taper angle. Little experimental scatter was found being the maximum for the dual adhesive joint without taper (standard deviation of 1.16 kN). The error bars are not represented in Figure 6 to improve clarity. Figure 6 demonstrates that the joint strength of the stiff adhesive (AV138) can be significantly increased by use of a taper angle. This effect is not as visible when a less stiff adhesive (2015) is used alone or in the taper. It can be seen that the stiffest adhesive has a peak around 45°, falling off immediately after (Figure 6). The gain of performance obtained for AV138 for the 45° taper is of 33% in relation to the taperless configuration. 2015 and 2015 + AV138 have almost identical distributions, owing to the fact that it is the adhesive in the taper of the joint (2015) that dictates the effectiveness of the taper. In these two cases it is the same adhesive, so similar distributions are expected. Another interesting fact is the synergetic combination of adhesives in the taperless configuration (90°) (see Figure 6). Here, it can be seen that the combination of adhesives is stronger than either of the adhesives individually. This is explained by the sensitivity to stress risers

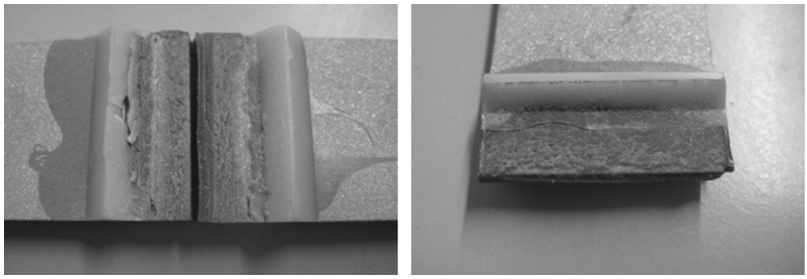

FIGURE 5 Fracture surfaces of mixed adhesive joints with a taper.

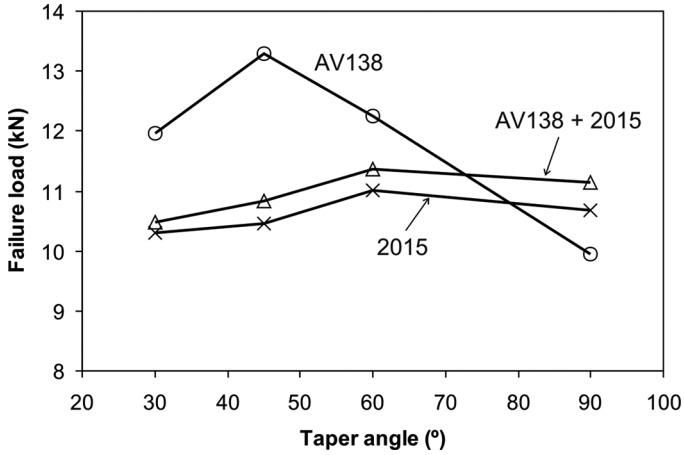

FIGURE 6 Joint strength evolution with taper angle.

of the AV138 adhesive due to its high stiffness and brittleness. This is a very stiff and strong adhesive, but performs badly in unfavourable conditions, such as the abrupt patch termination zone. When 2015 is placed in that area it resists better than AV138 would resist itself and the result is a joint better than any of the adhesives alone could provide.

A clip gauge of 50 mm was mounted on the specimen to measure the load displacement curves of the joints. The nonlinear behaviour of the

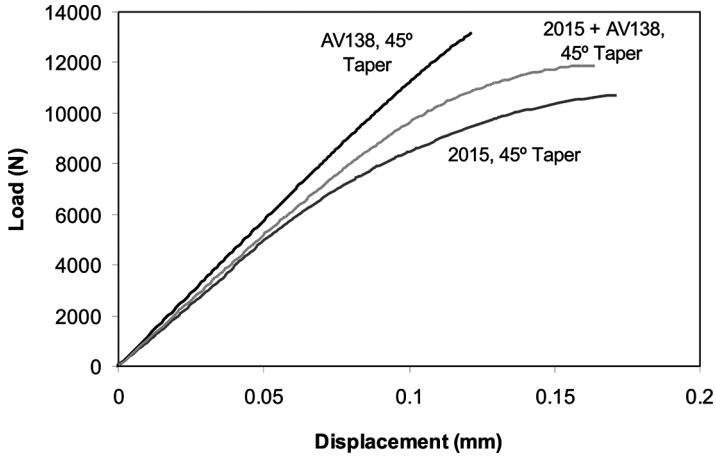

FIGURE 7 Load-displacement curves for joints with a 45° taper angle.

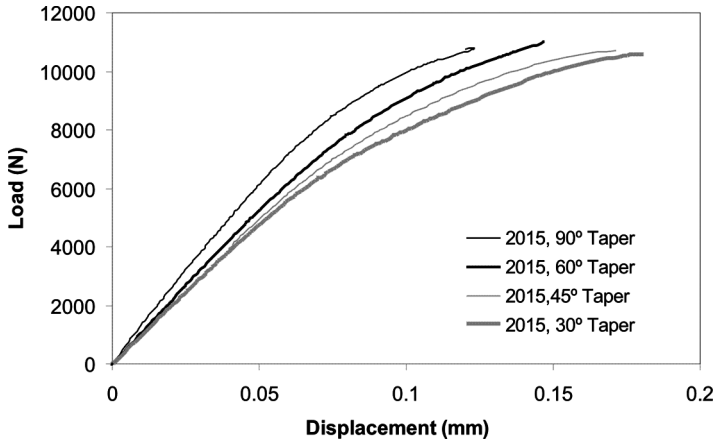

FIGURE 8 Load-displacement curves for joints with adhesive 2015 and various taper angles.

joints with 2015 is clearly visible, as shown in Figure 7. The taper and the spew fillet give a less rigid joint at the ends of the overlap and this effect is also captured in the load displacement curves, as shown in Figure 8.

Despite the fact that joints with AV138 alone and a taper of 45° are the strongest joints, the dual adhesive system might be more appropriate when a compromise of strength and ductility is sought. The flexible and ductile adhesive at the ends of the overlap gives a higher capacity to deform and is less sensitive to defects such as cracks. Applications where dynamic loadings such as fatigue or impact loads are frequent is an example where the use of dual adhesives might be more appropriate than reducing the stress levels by geometry modifications of a joint with a stiff adhesive.

4. JOINT MODELLING

The simulation work used the ABAQUS 6.6–3 program (Hibbit, Karlsson and Sorensen, Pawtucket, RI, USA). Elastic analyses were performed for all taper and adhesive combinations to asses the stress distribution in the different types of joints. Plastic analyses were carried out in order to understand the failure mechanism. In the case of the plastic analysis, the Drucker-Prager model was used [20].

A displacement of 0.5 mm was applied for the elastic analysis in all cases. Even though the level of stress is above the adhesive failure stress in the elastic analysis, it is adequate for comparison purposes.

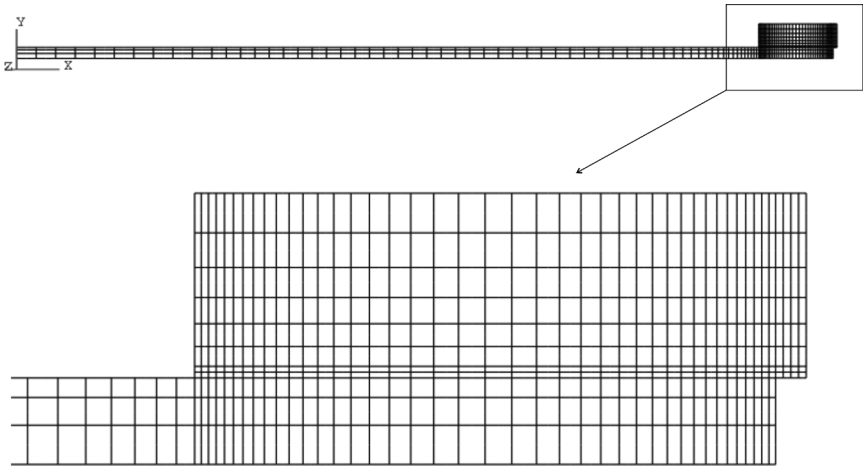

FIGURE 9 Typical mesh used in the finite element analysis of the double strap joints.

The mesh used was composed of CPE8R elements, which are 8-node bi-quadratic plane strain quadrilateral elements, with reduced integration to enable faster calculation. Each element was 0.2 mm long. A general aspect of the mesh can be seen in Figure 9. One quarter of the specimen was used to save computer power. A comparative analysis was made with different meshes of different resolutions. It was found that the stress distributions for this mesh were very similar to those obtained with meshes with the double of the density. For simplicity and faster processing times the simpler mesh was selected.

4.1. Elastic Analysis

Von Mises equivalent stress was chosen for this analysis as it encompasses all of the different stresses in the different directions acting on the adhesive. A von Mises stress distribution allows a quick and relevant assessment of the stress state in the joint. To choose the location of the path, a small parametric study was made. Stress distributions for three different locations in 45° tapered patch specimen were obtained in ABAQUS as shown in Figure 10. This figure shows that the differences are very small for the three locations. Based on this data it was decided to use the middle path for simplicity reasons.

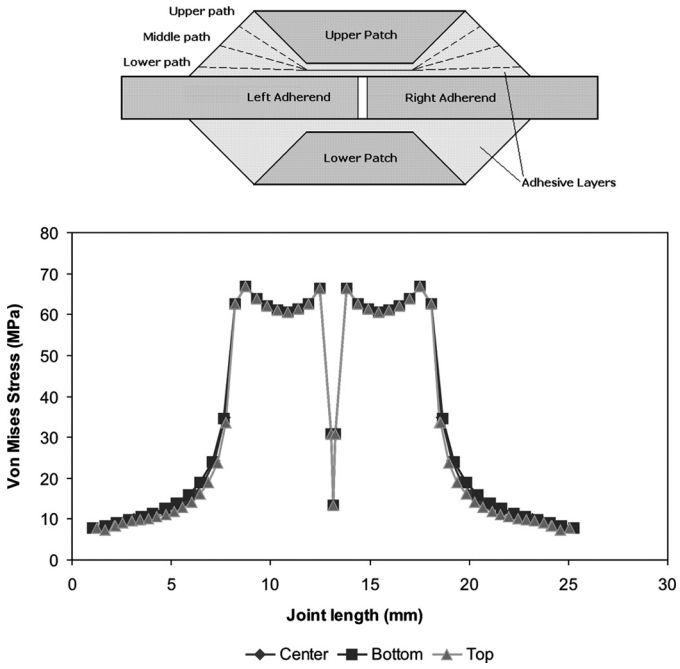

FIGURE 10 Von Mises stress for different path locations (adhesive 2015).

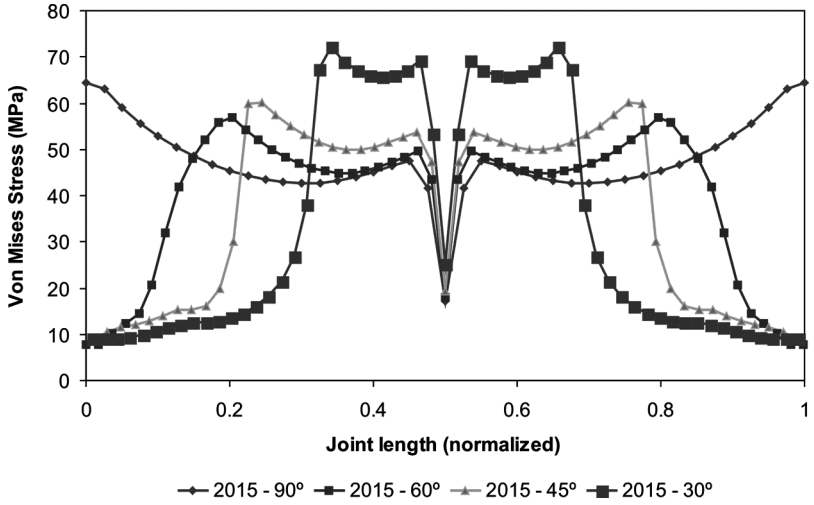

FIGURE 11 Von Mises stress distributions for 2015 adhesive models.

Figure 11 shows the von Mises stress distribution for Araldite 2015 adhesive ($E = 1850$ MPa). It shows that in the absence of a taper the stresses at the end of the patch are extremely high and concentrated. This is obviously the worst case scenario. The use of taper angles immediately lowers the tip (end of the patch) stresses to near zero. As the taper becomes longer and less steep, the loads are transferred to the centre section. Extremely low taper angles bring excessive stress to the centre section and offer lower joint strength. The ideal angles in this configuration are 60° and 45°. They combine smooth stress distribution at the tips with stresses in the centre that are close to those offered by the 90° configuration.

Figure 12 shows the von Mises stress distributions for AV138 ($E = 4590$ MPa). In the case of the 90° (no taper), the maximum stress is 40% higher than for the other configurations. This demonstrates that the taper angle is much more useful in stiff adhesives. The optimal taper angles for this case still appear to be the 45° and 60° configurations which are very closely matched and similar. It is interesting to note that at the tip of the taper the stresses for all angles are higher than observed for Araldite 2015 (see Figure 11).

The last case studied is depicted in Figure 13 and shows the combination of the two adhesives represented in the previous graphs. The stiffer adhesive (AV138) is placed in the centre of the joint while

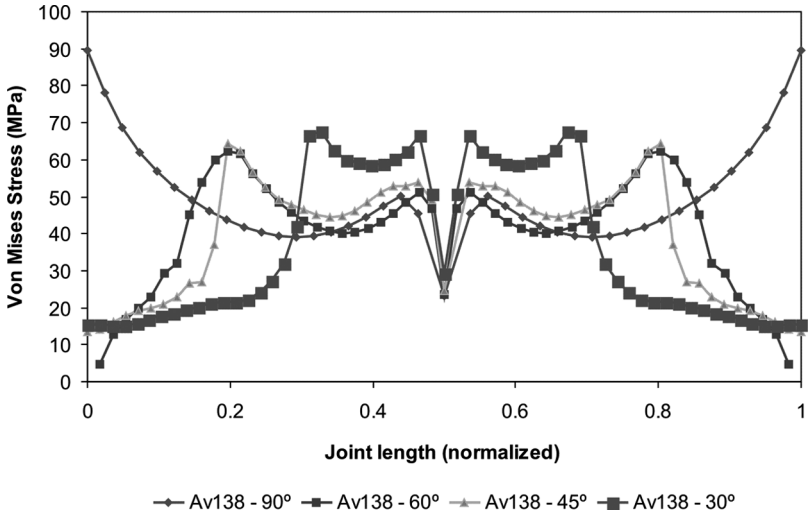

FIGURE 12 Von Mises stress distributions for AV138 adhesive models.

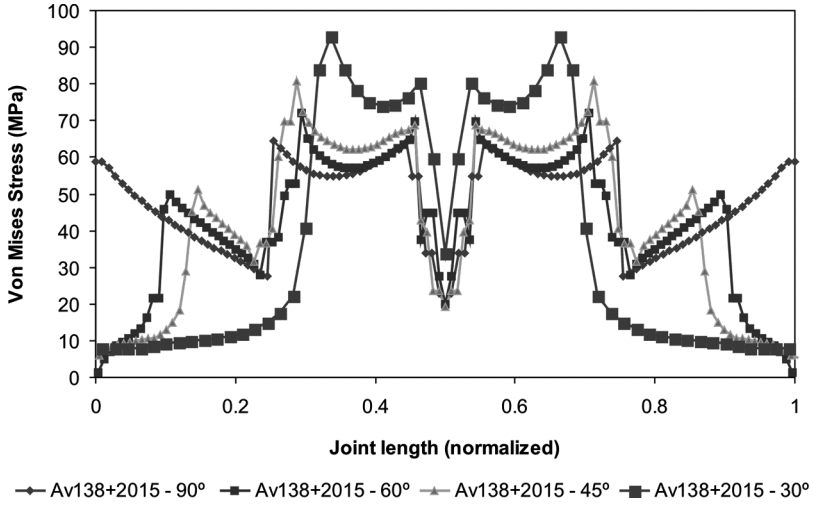

FIGURE 13 Von Mises stress distributions for dual adhesive models.

2015 is placed in the taper. This assures lower stresses at the tip, leading to smaller stress concentration. For the 90° case (no taper), it can be seen that the tip stress is identical to that observed using 2015 alone, but using a stronger adhesive in the centre section will almost certainly result in a stronger joint. This fact, among others in the graph, shows that the stress distribution of the adhesive combination is, in fact, an assembly of the individual distributions of each adhesive. If necessary, a joint can be engineered with specific stress distributions by combining sections of different adhesives and controlling their length.

4.2. Plastic Analysis

The plastic behaviour of the adhesive was modelled using the exponent Drucker-Prager criterion [20] which takes into account the hydrostatic stress. There are other models that include the first stress invariant such as the one of Raghava *et al.* [21] and the one of Dolev and Ishai [22]. The Raghava and the exponent Drucker-Prager criteria are equivalent when the exponent parameter (b) is 2. The yield criterion can be expressed as:

$$aq^b - p = p_t. \tag{3}$$

TABLE 2 Drucker-Prager Parameters

Parameter	2015	AV138/HV998
b	2	2
λ	1.4	1.3
a	0.041	0.03045

The terms that appear in Equation 3 are defined as:

$$a = \frac{1}{3(\lambda - 1)\sigma_{yt}}$$

$$q = \sqrt{\frac{1}{2}[(\sigma_1 - \sigma_2)^2 + (\sigma_2 - \sigma_3)^2 + (\sigma_3 - \sigma_1)^2]} = \sqrt{3J_2}$$

$$b = 2$$

$$p = -\frac{1}{3}(\sigma_1 + \sigma_2 + \sigma_3) = -\frac{1}{3}I_1$$

$$p_t = \frac{\lambda\sigma_{yt}}{3(\lambda - 1)},$$

where λ is the ratio of yield stress in compression to the yield stress in tension, $\sigma_i (i = 1, 2, 3)$ are the principal stresses, σ_{yt} is the yield stress in

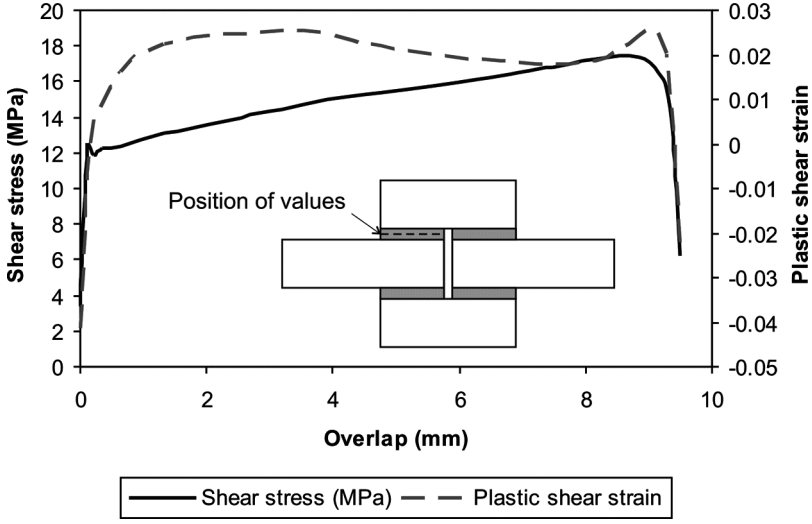

FIGURE 14 Shear stress and plastic shear strain distribution for the adhesive 2015 at the experimental failure load.

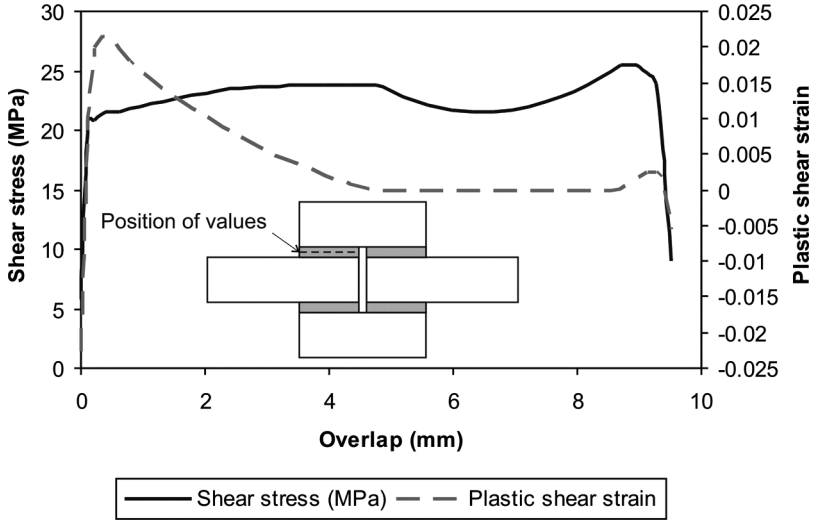

FIGURE 15 Shear stress and plastic shear strain distribution for the adhesive AV138 at the experimental failure load.

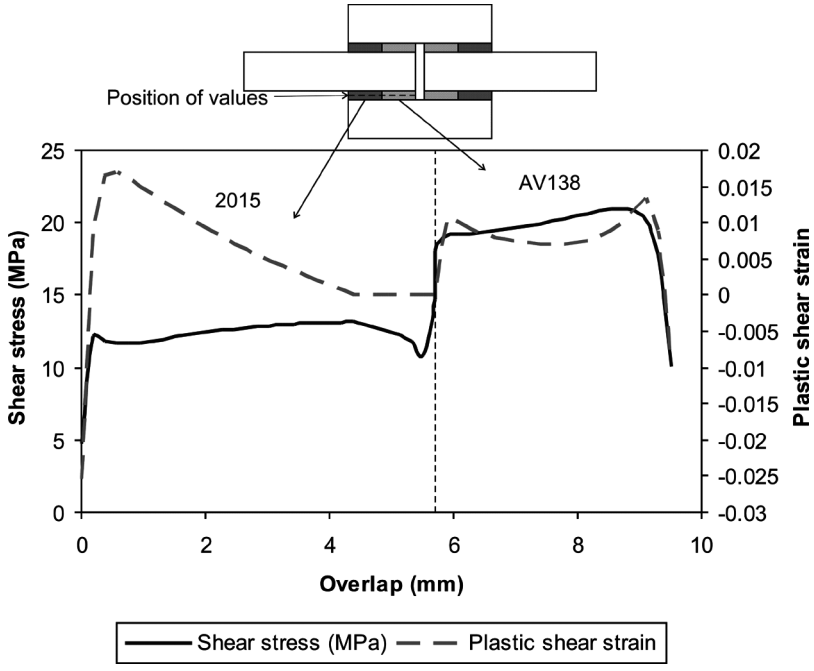

FIGURE 16 Shear stress and plastic shear strain distribution for the mixed adhesive joint (AV138 + 2015) at the experimental failure load.

tension, J_2 is the second deviatoric stress invariant, and I_1 is the first invariant of the stress tensor. Note that when $\lambda = 1$, the exponent Drucker-Prager model is equivalent to the von Mises criterion. The model of Drucker-Prager requires data from compression and tensile testing to calculate the λ ratio. An alternative method can be used to enable calculation with tensile and shear test results. Adhesive 2015 was tested in shear using the Thick Adherend Shear Test (TAST) (ISO 11003-2), so this technique is very appropriate for this case. To find the parameters that correctly model the adhesive, a comparative method is needed. Comparisons were performed between finite element analysis models and actual test results. Finite element models loaded with tensile test data were subjected to a pure shear load, from which one can obtain a shear stress-strain distribution. By varying the parameters of the variables in the Drucker-Prager criterion, one can obtain a series of shear stress-strain distributions and compare them with the actual experimental TAST test results. The λ ratio obtained by this method is indicated in Table 2. The Drucker-Prager

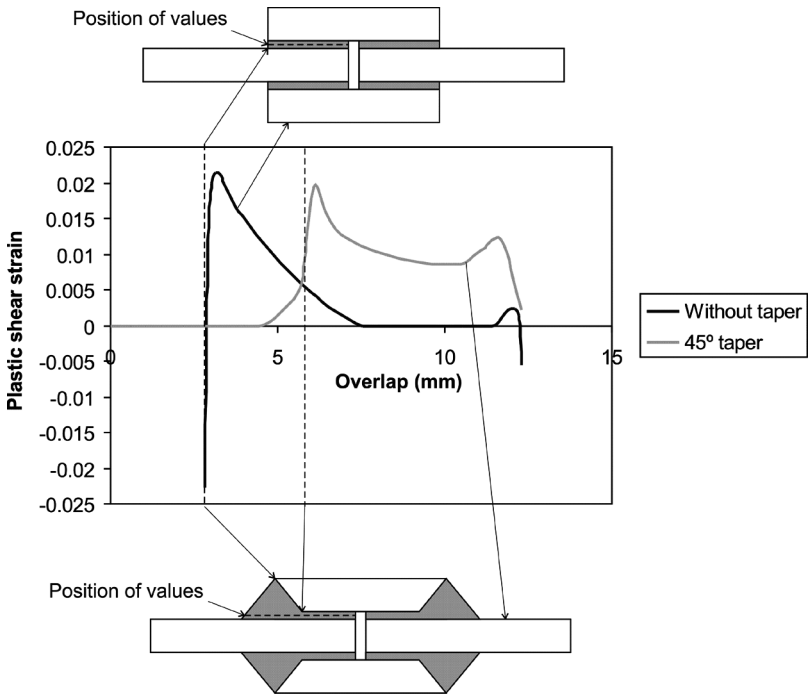

FIGURE 17 Plastic shear strain distribution at failure load for adhesive AV138 with a 45° taper and without taper.

exponential parameters for adhesive AV138 were gathered from literature [23] and are also listed in Table 2.

For the case of the joints without taper (90° case), the plastic analysis shows that for adhesive 2015 the failure occurs due to global yielding of the adhesive, *i.e.*, when all the overlap has yielded. A load corresponding to the experimental failure load was used in the finite element modelling. The shear stress and strain distributions along the overlap presented in Figure 14 show that the adhesive has yielded completely. In the case of the more brittle adhesive AV138, the shear stress and strain distributions along the overlap presented in Figure 15 show that the failure occurs when the strain reaches the failure strain of the adhesive (corresponding to a plastic strain of 0.02). In this case, the adhesive is not sufficiently ductile and the failure occurs before the adhesive has yielded along all of the overlap. In the case of mixed adhesive joints (see Figure 16), the overlap corresponding to AV138 is shorter and the adhesive can this time yield

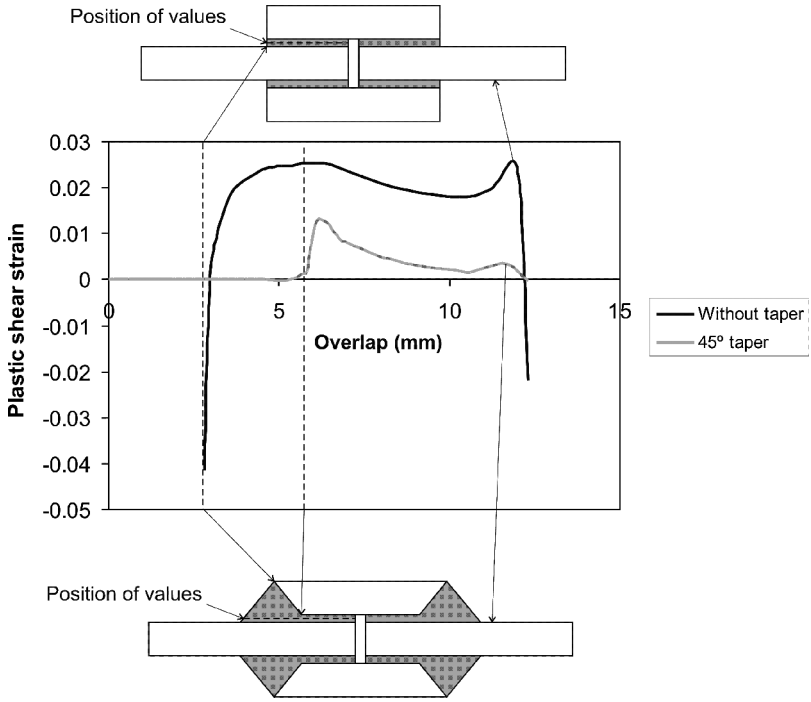

FIGURE 18 Plastic shear strain distribution at failure load for adhesive 2015 with a 45° taper and without taper.

completely. In this case, the whole overlap is at yield which means that both adhesives give their maximum load bearing capacity. This explains why for joints with no taper, the mixed adhesive joint is stronger than the joints with only one adhesive.

The taper has a strong effect on the brittle adhesive AV138. The taper decreases the strength of the singularity at the ends of the overlap decreasing, therefore, the level of stress. With a taper, the brittle adhesive AV138 fails not because it reaches its adhesive failure strain but because the whole overlap has yielded (adhesive global yielding) (see Figure 17). In the case of a taper, once the overlap corresponding to the inner part with the thinnest and constant bondline yields completely, the remaining adhesive area located beneath the taper is not sufficiently strong to support any more load, causing joint failure. With a taper, adhesive AV138 can sustain a higher load and makes more use of the overlap. In the case of the more ductile adhesive 2015, the ductility of the adhesive compensates for the strong singularity of the 90° case (no taper) which makes this adhesive practically not sensitive to any stress riser. With or without taper, the adhesive can yield along all the overlap, as shown in Figure 18.

5. CONCLUSIONS

Aluminium double lap (or patches) specimens with internal taper and dual adhesives were analysed with the finite element method and tested experimentally. The main conclusions are:

1. A taper angle of 45° reduces stresses at the end of the patch.
2. Tapered patches are more adequate for stiff adhesives, providing up to 30% stronger joints.
3. The combination of a ductile adhesive (2015) and a brittle adhesive (AV138) has a synergetic effect in taperless configurations.
4. Joints with dual adhesives have a strength comparable with that of joints with a stiff adhesive alone and are at the same time more flexible and ductile. This can be useful, especially for dynamic loadings.

REFERENCES

[1] Hu, F. Z. and Soutis, C., *Composites Science and Technology* **60**, 1103–1114 (2000).
[2] Adams, R. D., Atkins, R. W., Harris, J. A., and Kinloch, A. J., *J. Adhesion* **20**, 29–53 (1986).
[3] Hildebrand, M., *Int. J. Adhes. Adhes.* **14**, 261–267 (1994).
[4] Rispler, A. R., Tong, L., Steven, G. P., and Wisnom, M. R., *Int. J. Adhes. Adhes.* **20**, 221–231 (2000).

[5] Guild, F. J., Potter, K. D., Heinrich, J., Adams, R. D., and Wisnom, M. R., *Int. J. Adhes. Adhes.* **21**, 435–443 (2001).
[6] Belingardi, G., Goglio, L., and Rossetto, M., *Int. J. Adhes. Adhes.* **25**, 173–180 (2002).
[7] Kaye, R. H. and Heller, M., *Int. J. Adhes. Adhes.* **22**, 7–21 (2002).
[8] Amijima, S. and Fujii, T., *Int. J. Adhes. Adhes.* **9**, 155–160 (1989).
[9] Sancaktar, E. and Nirantar, P., *J. Adhesion Sci. Technol.* **17**, 655–675 (2003).
[10] Vallée, T. and Keller, T., *Compos. Part B-Eng.* **37**, 328–336 (2006).
[11] da Silva, L. F. M. and Adams, R. D., *Int. J. Adhes. Adhes.* **27**, 227–235 (2007).
[12] Sancaktar, E. and Kumar, S., *J. Adhesion Sci. Technol.* **14**, 1265–1296 (2000).
[13] Pires, I., Quintino, L., Durodola, J. F., and Beevers, A., *Int. J. Adhes. Adhes.* **23**, 215–223 (2003).
[14] Fitton, M. D. and Broughton, J. G., *Int. J. Adhes. Adhes.* **25**, 329–336 (2005).
[15] Temiz, S., *J. Adhesion Sci. Technol.* **20**, 1547–1560 (2006).
[16] Bouiadjra, B. B., Fekirini, H., Belhouari, M., Boutabout, B., and Serier, B., *Comp. Mater. Sci.* **40**, 20–26 (2007).
[17] da Silva, L. F. M. and Adams, R. D., *Int. J. Adhes. Adhes.* **27**, 362–379 (2007).
[18] da Silva, L. F. M. and Adams, R. D., *Int. J. Adhes. Adhes.* **27**, 216–226 (2007).
[19] Alcoa, Aluminium Alcoa 6063 Datasheet, http://www.asminternational.org/pdf/datasheets/al392.pdf
[20] Drucker, D. C. and Prager, W., *Quart. Appl. Math.* **10**, 157–165 (1952).
[21] Raghava, R. S., Cadell, R., and Yeh, G. S. Y., *J. Mater. Sci.* **8**, 225–232 (1973).
[22] Dolev, G. and Ishai, O., *J. Adhesion* **12**, 283–294 (1981).
[23] da Silva, L. F. M., Rodrigues, T. N. S. S., Figueiredo, M. A. V., de Moura M. F. S. F., and Chousal, J. A. G., *J. Adhesion* **82**, 1091–1115 (2006).